Synthetic cation-selective nanotube: Permeant cations chaperoned by anions

Tamsyn A. Hilder,[a] Dan Gordon, and Shin-Ho Chung
Computational Biophysics Group, Research School of Biology, Australian National University, Canberra, ACT 0200, Australia

(Received 23 July 2010; accepted 12 November 2010; published online XX XX XXXX)

The ability to design ion-selective, synthetic nanotubes which mimic biological ion channels may have significant implications for the future treatment of bacteria, diseases, and as ultrasensitive biosensors. We present the design of a synthetic nanotube made from carbon atoms that selectively allows monovalent cations to move across and rejects all anions. The cation-selective nanotube mimics some of the salient properties of biological ion channels. Before practical nanodevices are successfully fabricated it is vital that proof-of-concept computational studies are performed. With this in mind we use molecular and stochastic dynamics simulations to characterize the dynamics of ion permeation across a single-walled (10, 10), 36 Å long, carbon nanotube terminated with carboxylic acid with an effective radius of 5.08 Å. Although cations encounter a high energy barrier of 7 kT, its height is drastically reduced by a chloride ion in the nanotube. The presence of a chloride ion near the pore entrance thus enables a cation to enter the pore and, once in the pore, it is chaperoned by the resident counterion across the narrow pore. The moment the chaperoned cation transits the pore, the counterion moves back to the entrance to ferry another ion. The synthetic nanotube has a high sodium conductance of 124 pS and shows linear current-voltage and current-concentration profiles. The cation-anion selectivity ratio ranges from 8 to 25, depending on the ionic concentrations in the reservoirs. © *2010 American Institute of Physics*. [doi:10.1063/1.3524310]

I. INTRODUCTION

Interest in designing ion-selective, nanoscale pores using synthetic nanotubes to broadly mimic some of the functions of biological ion channels is rapidly gaining momentum. Engineered ion channels, once successfully designed and fabricated, will have numerous potential applications, such as antimicrobial agents, ultrasensitive sensors, and reverse osmosis membranes. Theoretical and experimental studies thus far have mainly focused on nanotubes which can mimic the biological water channel, aquaporin.[1–7] These synthetic water channels have flow rates substantially higher than both aquaporin and currently-used desalination membranes. Recently, ion-selective nanotubes made from carbon atoms and boron and nitrogen atoms have been successfully designed.[8–13] By placing a rim of partially charged atoms near the entrance, carbon nanotubes can be made to be selectively permeable to anions[14] or their interior can be made hospitable specifically to cations or anions.[9] Similarly, Hilder *et al.*[12] and Won and Aluru[13] have shown ionic selectivity of boron nitride nanotubes. Recently, Lee *et al.*[15] successfully fabricated single-wall carbon nanotube ion channels 1.5 nm in diameter and with negatively charged ends that are capable of selectively conducting protons. By subsequent blocking of larger cations they demonstrate the possibility of a single-ion detection device.

It is now possible to fabricate carbon nanotubes with either hydroxyl (-OH), carbonyl (O=C), or carboxylic acid (-COOH) functional groups attached to the end.[1,16] Such functionalized nanotubes are commercially available, have high solubility,[17,18] and are stable when embedded in a lipid bilayer.[19] For engineered nanotubes to have practical biological applications, their radii must be small and be comparable to those found in biological ion channels and their length must be approximately equal to the thickness of a lipid bilayer. Moreover, the tubes should spontaneously insert across[19] and remain stable in[14] the cell membrane. Once such synthetic nanotubes meeting all these criteria are found, they can be targeted to certain cell types by attaching specific antibodies or otherwise.

Before practical nanoscale devices which possess the functionality of biological channels can be successfully created and widely utilized, proof-of-concept computational studies must be performed. With this aim in mind, we have carried out computational studies on a functionalized carbon nanotube, using molecular dynamics calculations and stochastic dynamics simulations. Specifically, we examine the conductance properties of a (10, 10) carbon nanotube, whose effective radii and length are, respectively, 5.08 and 36 Å, terminated with carboxylic acid functional groups.

II. COMPUTATIONAL DETAILS

We perform molecular dynamics (MD) and distributional molecular dynamics (DMD) simulations on a (10, 10) carbon nanotube terminated with carboxylic acid (-COOH) as shown in Fig. 1(a) embedded in a lipid bilayer separating two reservoirs [Fig. 1(b)]. The latter computational method combines

[a]Author to whom this correspondence should be addressed. Electronic mail: tamsyn.hilder@anu.edu.au.

 © 2010 American Institute of Physics

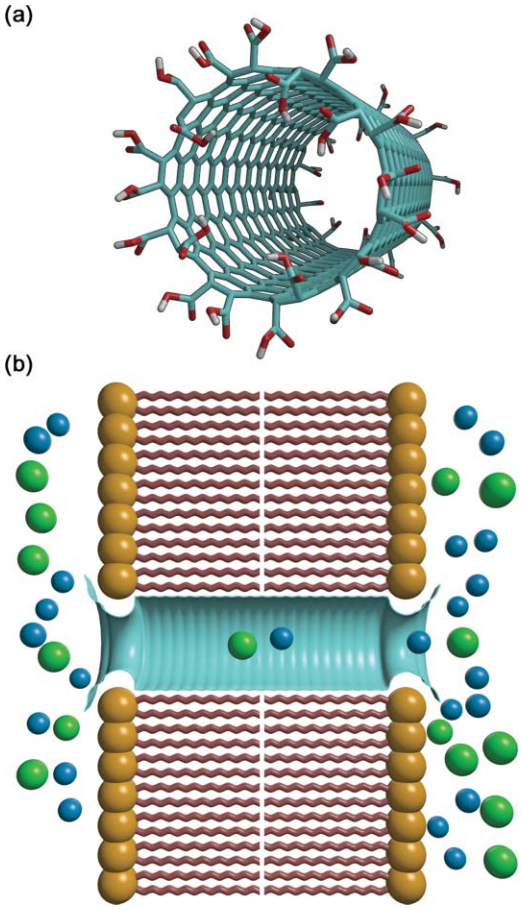

FIG. 1. Schematic illustration of (a) the (10, 10) carbon nanotube with carboxylic acid terminated ends, and (b) the simulation assembly used in DMD, composed of reservoirs containing charged particles and the nanotube embedded in a lipid bilayer. For clarity, not all ions in the reservoir are shown. Sodium ions are shown in blue, and chloride ions in green.

molecular and stochastic dynamics to reproduce the distribution of ion trajectories implicit in MD as closely as possible while measuring ion permeation at much longer timescales than possible with MD.[20] For more detail on the methods, we refer the reader to our previous papers.[14,20,21]

A. Nanotube construction

Single-walled (10, 10) carbon nanotubes are constructed from a hexagonal array of carbon atoms rolled up to form a cylinder with the physical properties given by Dresselhaus *et al.*[22] and a carbon-carbon bond distance of 1.42 Å.[22] The etching process involved in fabricating open-ended nanotubes introduces either hydroxyl (-OH), carbonyl (C=O), or carboxylic acid (-COOH) functional groups to the nanotube ends.[16] Therefore, in this paper the nanotubes are terminated with carboxylic acid (-COOH) functional groups, as illustrated in Fig. 1(a). The Lennard–Jones parameters for the COOH group are taken from the CHARMM27 force field[23] and partial charges obtained from Zheng *et al.*[24] Specifically, the partial charges for the COOH group are as follows:[24] C (on nanotube) (0.08 e), C (0.55 e), =O (-0.50 e), O (-0.58 e), and H (0.45 e) so that the nanotube (including its carboxylic acid terminated ends) are overall neutral.

It is not clear at what pH experimental measurements should be carried out to replicate the theoretical calculations we describe here. As the pK_A value of the carboxylic group is near 4, the terminated ends are expected to be deprotonated in bulk, neutral solutions. If all carboxyl terminals are deprotonated and the (10, 10) nanotube becomes terminated with COO^-, we expect the tube to be permeable predominantly to cations. In reality, the situation is somewhat complicated in a mesoscopic system. When ionized residues are located in close proximity (~4–12 Å), pK values of individual residues are known to shift away from those determined in bulk solutions.[25,26] For example, the pK_A value of four sidechains of the glutamic acids (E118) guarding the intracellular gate of the KcsA potassium channel is calculated to be 6.9, compared to the model pK_A value of 4.4.[25] Thus, the degree of deprotonation in our COOH-terminated nanotube at various pH needs to be calculated by using macroscopic electrostatics or otherwise, and this issue deserves further theoretical investigation. One of the ways to avoid this uncertainty would be to replace the carboxylic functional group in the nanotube with a simple ester, such as CO_2CH_3.

Carbon nanotubes are defined by their chiral vector $\boldsymbol{C} = n\boldsymbol{a_1} + m\boldsymbol{a_2} = (n, m)$, *where* $\boldsymbol{a_1}$ *and* $\boldsymbol{a_2}$ represent the unit vectors of the hexagonal lattice and n and m are integers. We consider only an armchair type nanotube which is defined as (n, n). In particular, we investigate (10, 10) carbon nanotubes with an effective radius of 5.08 Å, and a length of approximately 36 Å. It is now technically feasible to fabricate nanotubes of this radii, and nanotubes with these functional groups (COOH) are readily available online, for example through CheapTubes Inc. (www.cheaptubesinc.com) or NanoLab Inc. (www.nano-lab.com). Although these diameter nanotubes with COOH terminated ends are available online their lengths are long compared to our simulation. We require lengths of 3.6 nm, whereas the shortest length available online is 0.5 μm. Therefore, to fabricate nanotubes such as those proposed here it will be necessary to shorten their length, using the procedures detailed elsewhere.[27,28]

B. Molecular dynamics simulations

Molecular dynamics simulations are conducted using NAMD,[29] visualized using VMD,[30] with the CHARMM27 force field[23] and TIP3P water model. The MD domain consists of the carbon nanotube embedded in a POPE lipid bilayer separated by two reservoirs, as illustrated in Fig. 1(b). The system is replicated in all three dimensions and particle mesh Ewald electrostatics is used. The simulation box is approximately 64 × 64 × 79 $Å^2$, and contains 3953 water molecules and either 1 sodium or 1 chloride ion. The center-of-mass of the nanotube is constrained to allow for tilting of the nanotube, and the nanotube axis is used as the reaction coordinate to measure ion trajectories. No constraints are applied to the lipid bilayer. Each system is equilibrated for 1 ns at a constant temperature of 310 K and a constant pressure of 1 bar.

The three-dimensional potential of mean force (PMF) or free energy is constructed using umbrella sampling at an ionic

concentration of 0 mM. In other words, only the ion of interest is present in the simulation. This enabled the three-dimensional PMF to be used directly in subsequent DMD simulations while avoiding double counting the ion-ion interactions in subsequent DMD simulations, in which the ion-ion interactions are explicitly dealt with using macroscopic electrostatics.[14] As a result of including only the ion of interest, the system will have a non-neutral charge. With particle mesh Ewald electrostatics this results in a homogeneous neutralizing background charge filling the entire simulation space.[31] Although this will affect the free energy due to the interaction of solute charges with their own periodic copies and the neutralizing background charge, its effect is negligible for a non-neutral charge of ± 1 e. As mentioned the nanotube and its terminated ends are overall neutral.

Given that the nanotube is symmetric, the ion positions are sampled only in the positive z domain, and reflected to obtain the negative z PMF. Thus, the ion is moved through positions from 0 to 30 Å in steps of 0.5 Å and the z-component is held using a constraint of 12.5 kcal mol^{-1} Å^{-2}, while the ion is free to move radially. The harmonic constraint is chosen to give adequate overlap between each window while constraining the ion enough to ensure sufficient sampling. The ion's z and r coordinates are obtained during each umbrella sampling run of 1 ns, and runs are analyzed using the weighted histogram analysis method[32] to obtain a two-dimensional PMF with the reaction coordinates (z, r). This two-dimensional PMF is converted thermodynamically into a three-dimensional, radially symmetric PMF as follows. Letting $U_3(z, r, \theta) = U_3(z, r)$ be the three-dimensional, radially symmetric PMF and $U_2(z, r)$ be the two-dimensional cylindrical PMF, we have[33]

$$\exp\left(\frac{-U_2(z,r)}{kT}\right) = C_1 \int_0^{2\pi} r \exp\left(\frac{-U_3(z,r)}{kT}\right) d\theta = 2\pi r C_1 \exp\left(\frac{-U_3(z,r)}{kT}\right), \quad (1)$$

where C_1 is an arbitrary constant that sets the zero point of the energy. We then obtain, to within an arbitrary constant,

$$U_2(z,r) = U_3(z,r) - kT \ln(r). \quad (2)$$

Thus, the three-dimensional, radially symmetric PMF can be obtained from the two-dimensional cylindrical PMF by adding an offset proportional to the log of the radial coordinate.

C. Distributional molecular dynamics

The conductance of the nanotube should ideally be determined using MD which uses an explicit solvent, but it is not feasible computationally to construct a current-voltage-concentration profile using this method. To overcome these difficulties for modeling the permeation of ions across a nanotube, we have devised a new methodology called DMD that combines molecular and stochastic dynamics[20] and uses an implicit solvent. The theoretical basis for this procedure and a detailed test using gramicidin-A are given by Gordon *et al.*[20]

To begin with, molecular dynamics is used to determine a free energy profile for the ion in the nanotube, and the distribution of random and frictional forces (friction kernel) is measured over discrete segments of the tube. By doing this we can match the distribution of ion trajectories in DMD as closely as possible to MD. These parameters are then used in stochastic dynamics simulations based on the nonlinear generalized Langevin equation given by

$$\begin{aligned} \partial_t \mathbf{q}(t) &= m^{-1}\mathbf{p}(t), \\ \partial_t \mathbf{p}(t) &= \mathbf{F_D}(\mathbf{q}(t)) - \int_0^t dt' K(t')\mathbf{p}(t-t') + \mathbf{F_R}(t), \end{aligned} \quad (3)$$

where $\mathbf{q}(t)$ and $\mathbf{p}(t)$ are the coordinate and momentum at time t, respectively, m is the mass, and $\mathbf{F_D}$ represents the deterministic force or in this case the PMF. The second term represents the frictional force in which $K(t')$ is the friction kernel. The last term $\mathbf{F_R}$ is the random force which is assumed to be a Gaussian random force related to the friction kernel through the fluctuation-dissipation theorem, which is given by

$$\left\langle \mathbf{F_R}(0)\mathbf{F_R^T}(t)\right\rangle = kT\,K(t)m. \quad (4)$$

The nonlinear generalized Langevin equation is solved using an extension of the leapfrog method as outlined in Gordon *et al.*[34] (further detail is also provided by Nilsson and Padró[35] and Wan *et al.*[36]).

In order to prevent double-counting of the interaction between any given ion and the net effect of all the other ions, we perform our molecular dynamics simulation at 0 mM to generate the PMF used in DMD. Preliminary work suggests that the PMF obtained from DMD at finite concentrations compares well with that obtained from MD. All ion-ion related effects are a result of the macroscopic electrostatics that are built into the stochastic simulation.

The simulation space is divided into (i) a channel region, where the nonlinear generalized Langevin Eq. (3) is solved with a 2 fs timestep using the free energy and friction kernel determined from MD; and (ii) the bulk region, where normal Brownian dynamics and macroscopic electrostatics are performed with a longer timestep of 100 fs. All single-ion deterministic forces are derived from the PMF taken from MD, which represent the interactions between a single ion and the nanotube/membrane system. In contrast, the ion-ion interactions are calculated using macroscopic electrostatics (Poisson's equation with a dielectric barrier defined by the nanotube/membrane system) and other fitted short-range ion-ion forces. This approach may ignore the effect of anisotropic permittivity of water within the channel demonstrated by Toghraee *et al.*[37] However, in our simulations the anisotropic behavior only applies to the ion-ion interaction as all single ion forces are derived from our preceding MD simulations. Therefore, it is expected that the effect of anisotropy on our results will be marginal. In most cases the ions reside on the central axis of the pore where the axial permittivity is equivalent to bulk water,[37] and therefore axial ion-ion interactions will be unaffected by the anisotropic behavior. We note that the value used in our simulations for the dielectric constant of water has been shown to compare well to the physiological conductance through biological potassium channels.[38]

In MD, the COOH ends are free to move. In DMD a rigid tube boundary generated from equilibrated MD is present, but this boundary is only applied as a dielectric boundary for the calculation of ion-ion interactions. In contrast, the interactions between single ions and the tube walls are determined by the PMF, which represents the time-averaged effect of the flexible tube on the ions.

As mentioned, the PMF was determined using WHAM.[32] The data gathered for the WHAM is also used to determine the friction kernel, $K(t)$. For each ion trajectory we determine the momentum autocorrelation function $C(t)$ and derive $K(t)$ using

$$\partial_t C = -\int_0^t K'(t-t')C(t')\,dt'. \tag{5}$$

The inverse velocity decay time due to friction γ is then determined as the time integral of $K(t)$ from $t = 0$ to $t = \infty$. Note that the diffusion coefficient, D can be determined using γ and the Einstein relation $D = kT/(m\gamma)$, where k is Boltzmann's constant, T is the temperature, and m is the mass. We then assume the friction kernel can be approximated by an exponential function, thus

$$K(t) = \gamma\kappa \exp(-\kappa t), \tag{6}$$

so as to determine the inverse decay time of the friction memory kernel, κ.

In summary, three parameters that feature in the generalized Langevin Eq. (3) are the deterministic force $\mathbf{F_D}$, the random force $\mathbf{F_R}$, and the frictional force $\mathbf{F_F}$. The latter two forces represent the stochastic force arising from random collisions of an ion with its surrounding molecules. In Brownian dynamics these parameters are estimated by solving Poisson's equation and by using the fluctuation-dissipation theorem. In DMD, the pore is divided into thin slices, and the forces acting on an ion and the diffusion coefficient in each section are obtained from a three-dimensional PMF and friction kernel determined from MD. This ensures that for a single ion certain properties of the trajectory in MD, such as the probability of finding an ion at a given position, will be reproduced in DMD. When there are two ions in the pore, the interactions between them are treated using macroscopic electrostatics. Poisson's equation is solved to determine the ion-ion interaction with the results for all possible configurations of the two ions being stored in a lookup table which is consulted throughout the simulation.[21]

All current-voltage curves were generated at an ionic concentration of 500 mM, and all current-concentration profiles were generated at a voltage of 200 mV. Voltage is applied across the membrane in DMD simulations. A uniform electric field is applied across the channel, equivalent to placing two voltage plates at a distance and applying a potential ($\pm$V) on each plate. Current was calculated using the formula $I = qn/\Delta t$, where n is the average number of ions that cross the membrane, q is the charge of the ion, and Δt is the simulation time of one run, which in our case is 0.8 μs. The numbers of ions crossing the membrane are counted in the simulation period of 0.8 μs, and the simulation was repeated 5 times. The average number of ions that cross the membrane and the standard error of the mean are determined from these five simulations. The starting configuration of ions in the simulation is generated randomly, and each simulation is given a different randomly generated distribution. No ions are present inside the channel at the beginning of the simulation.

III. RESULTS AND DISCUSSION

The free energy profiles encountered by sodium (Na^+) and chloride (Cl^-) as they traverse the (10, 10) carbon nanotube with its ends terminated with carboxylic acid suggests that the pore will be impermeable to charged particles. Figure 2 shows the free energy profiles at 0 mM ionic concentration of sodium and chloride ions as they traverse the (10, 10) carbon nanotube with carboxylic acid terminated ends. Displayed in the upper panel [Figs. 2(a) and 2(b) are the one-dimensional free energy profiles, obtained from the two-dimensional (z, r) PMF by thermodynamic integration, of sodium and chloride ions, respectively. The lower panel [Figs. 2(c) and 2(d)] shows the two-dimensional free energy contours generated from the three-dimensional PMF by taking a slice through the nanotube center. The upper panels of Fig. 2 are one-dimensional PMFs and do not simply represent the on-axis values from the lower panels of Fig. 2. Instead, they are integrations over all radial and angular values available to the ion into a single value for each z coordinate of the ion.[33] If $U_3(x, y, z)$ is the three-dimensional PMF and $U_1(z)$ is the one-dimensional PMF, then

$$U_1(z) = -kT \ln\left(L_0^{-2}\int dx\,dy[\exp(-U_3(x, y, z)/kT)]\right), \tag{7}$$

where L_0 is an arbitrary length scale which simply determines the zero point of the energy.

For sodium ions, there exists a free energy barrier of approximately 7 kT, as illustrated in Figs. 2(a) and 2(c). At the entrance and exit of the nanotube (at $z = \pm 16$ Å) there exist two attractive energy wells for sodium ions. From Fig. 2(a) this well appears as a slight dip, but for Fig. 2(c) the well is more distinct (purple region) and is approximately 6 kT.

Similarly, a chloride ion encounters a free energy barrier of approximately 7 kT, as illustrated in Fig. 2(b). However, unlike sodium, inside the nanotube chloride ions encounter a reduction in free energy well of approximately 4.5 kT, as illustrated in Fig. 2(d) (blue). Therefore, once inside the nanotube chloride ions encounter an energy barrier to exit of approximately 4.5 kT [Fig. 2(b)]. Just outside the nanotube entrance and exit (at $z = \pm 19$ Å) chloride ions encounter an energy well of 2 kT, as is evident in Fig. 2(b). From Fig. 2(d) this energy well is shown to occur approximately 4 Å from the nanotube central axis (dark blue). Just inside the nanotube entrance and exit (at $z = \pm 14$ Å) a chloride ion encounters an energy well of approximately 2 kT, which is shown as a slight dip in Fig. 2(b), and a distinct well in Fig. 2(d) (blue). However, in contrast to sodium the energy at the nanotube entrance increases rapidly as the chloride ion moves away from the axial center of the nanotube. As a result a chloride ion encounters a much narrower entrance to the nanotube than a sodium ion. The terminated ends of the nanotube (COOH groups) are

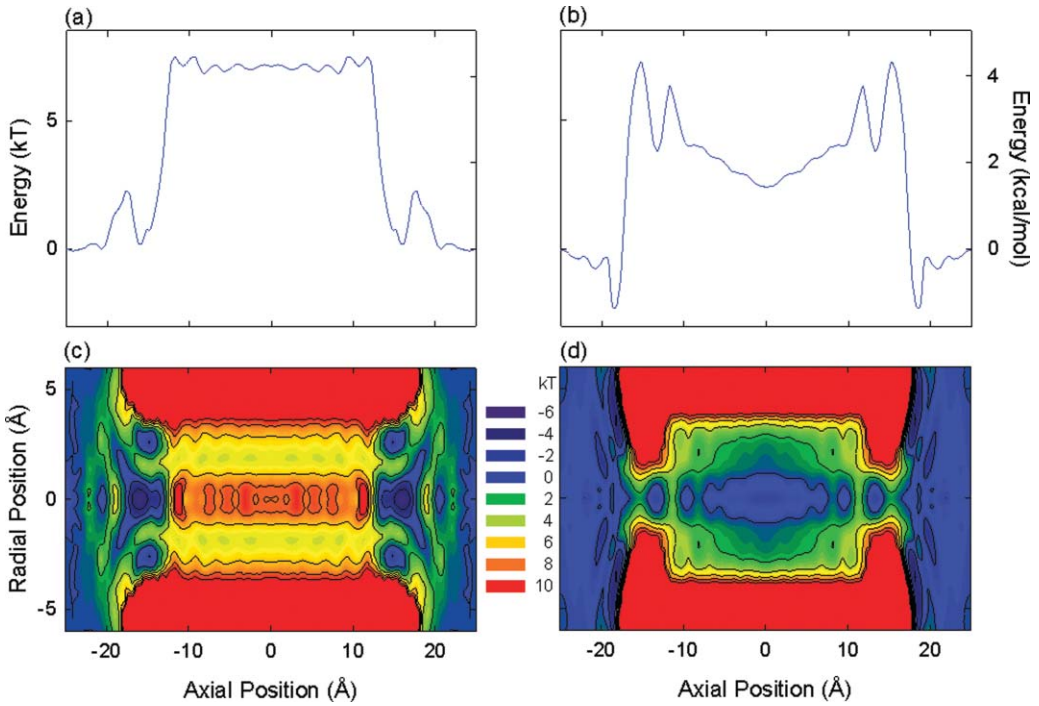

FIG. 2. Free energy of sodium (Na^+) and chloride (Cl^-) ions through the (10, 10) carbon nanotube with carboxylic acid terminated ends at 0 mM ionic concentration. Upper panel: one-dimensional free energy profile of (a) sodium and (b) chloride. Energy in the upper panel is given in units of kT (left-hand side) and kcal/mol (right-hand side). Lower panel: two-dimensional contour plot of the free energy landscape (kT) within the nanotube for (c) sodium and (d) chloride.

overall neutral and represent tight dipoles at the entrance and exit of the nanotube. Therefore, as expected the electric field decays quickly, as $1/R^3$.

Although the free energy barriers encountered by both the sodium and chloride ions are generally insurmountable, our simulations reveal that in fact substantial numbers of sodium ions move across the channel. As shown in Fig. 3(a), for sodium ions the current is 12 pA at an applied potential of 100 mV and ionic concentration of 500 mM. In contrast, for chloride ions the current is negligible at only 0.3 pA at 100 mV. By fitting a linear regression to the data points we obtain a large conductance of 124 ± 4 pS for sodium ions and 5 ± 0.6 pS for chloride ions. Alternatively, with an ionic concentration of 200 mM, the sodium and chloride current at 100 mV is 5.3 and 0.64 pA, respectively. On fitting a linear regression to the data points we obtain a conductance of 55 ± 2 pS for sodium ions and 7 ± 0.4 pS for chloride ions (data not shown). The chloride conductance remains a similar magnitude despite the reduction in ionic concentration from 500 to 200 mM. The energy well encountered by sodium ions at the nanotube entrance [Figs. 2(a) and 2(c)] acts to limit the number of chloride ions which can pass through the nanotube since for chloride ions to pass through the nanotube entrance they must follow the axial center of the nanotube.

Figure 3(b) shows the current-concentration profile of sodium ions. The current is shown to steadily increase with increasing ionic concentration following a linear relationship rather than that of Michaelis–Menten form. This suggests that the time spent by an ion waiting to enter the channel will decrease as the concentration increases. Even at high concentrations, the rate limiting step is the diffusion of ions into the channel.

To clarify how sodium ions can conduct across this nanotube despite an insurmountable energy barrier observed in Fig. 2 we examine the ion binding sites within the nanotube, how a resident ion transits from one binding site to another and study ion animations of the conduction process. We find that cations are able to move across the (10, 10) carbon nanotube pore only when they are chaperoned by chloride ions. At the nanotube entrance a resident sodium ion enables chloride to overcome the energy barrier and enter the nanotube interior. Once inside the nanotube these resident chloride ions act to ferry, or chaperone, sodium ions from the entrance to the exit of the nanotube. This artificial channel resembles that of the mutant glycine receptor[38] in which anions act to chaperone sodium ions[40,41] with a conductance of 17 pS.

We divide the nanotube length into 100 thin sections and compute time averages of both sodium and chloride ions in each section during the simulation period of 4 μs. In the absence of an applied potential, resident chloride ions tend to dwell within the nanotube and resident sodium ions tend to dwell at the pore entrances and within the nanotube, as shown in Fig. 4. On average, there are 1.7 chloride ions occupying the nanotube interior. In contrast, there are on average 0.7 sodium ions occupying the binding sites at the pore entrances, and 1.1 sodium ions occupying the channel interior. Although almost two chloride ions occupy the channel during the simulation the chloride conductance is considerably less than sodium, 5 pS compared to 124 pS, suggesting that chloride is acting to mainly chaperone sodium across the channel.

Detailed analysis of the dynamics of ion permeations reveals that translocation of sodium ions across the nanotube is indeed achieved by ion chaperoning. This process can be

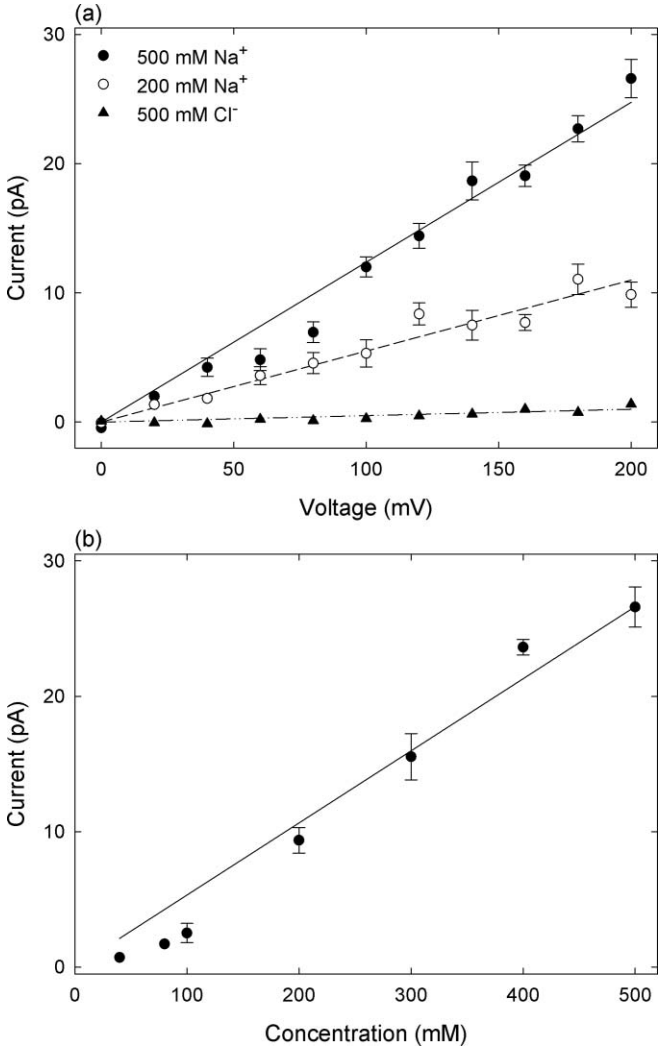

FIG. 3. Current-voltage-concentration profiles for the (10, 10) carbon nanotube with carboxylic acid terminated ends. (a) Current-voltage profile for sodium ions using an ionic concentration of both 200 (open circles) and 500 mM (filled circles), and chloride ions using an ionic concentration of 500 mM (filled triangles). (b) Current-concentration profile for sodium at an applied potential of 200 mV. Error bars represent one standard error of the mean, and error bars smaller than the data points are not shown.

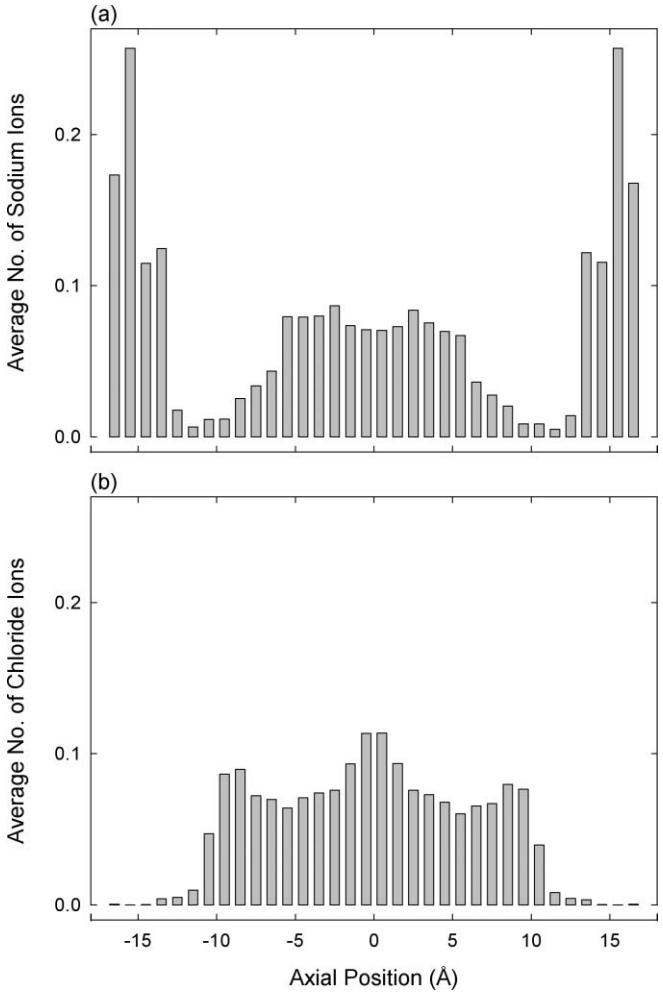

FIG. 4. Binding sites for (a) sodium and (b) chloride ions for the (10, 10) carbon nanotube with carboxylic acid terminated ends in the absence of an applied potential and at an ionic concentration of 500 mM.

observed in DMD animations (snapshot is shown in Fig. 5) in which a resident chloride ion acts to ferry sodium ions from the entrance to the exit of the nanotube. We can also detail this process by recording the axial position of every ion in the pore at each timestep under the influence of an applied potential of 100 mV and at an ionic concentration of 500 mM. These positions can then be used to determine the ion configuration within the nanotube. Initially sodium ions occupy the two binding sites at the nanotube entrance and exit. These sodium ions enable a chloride ion to overcome its energy barrier and enter the nanotube interior. However, this event takes on average 50 ns. A chloride ion then occupies the nanotube interior for the remainder of the simulation. Sodium ions can only enter the nanotube interior when the resident chloride is present. Therefore, for the first 50 ns of simulation no sodium ions are present in the nanotube interior. Sodium ions then occupy at least one binding site for the remainder of the simulation. In fact, for 72% of the simulation time a sodium ion occupies an entrance and/or exit binding site and the nanotube interior.

The presence of a chloride ion in the pore lowers the energy barrier encountered by the sodium ion. Figure 6 illustrates how a resident chloride ion, fixed at the nanotube

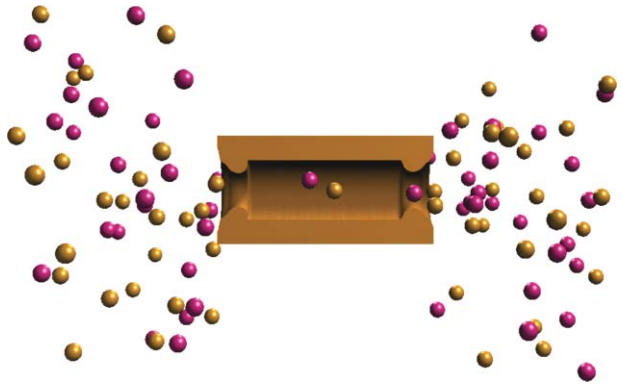

FIG. 5. A segment of video animation from DMD simulations showing a resident chloride ion (gold) which acts to chaperone sodium ions (pink) from entrance (left) to exit (right) of the pore (enhanced online). For clarity the nanotube is shown as a bronze surface with half of the channel removed.

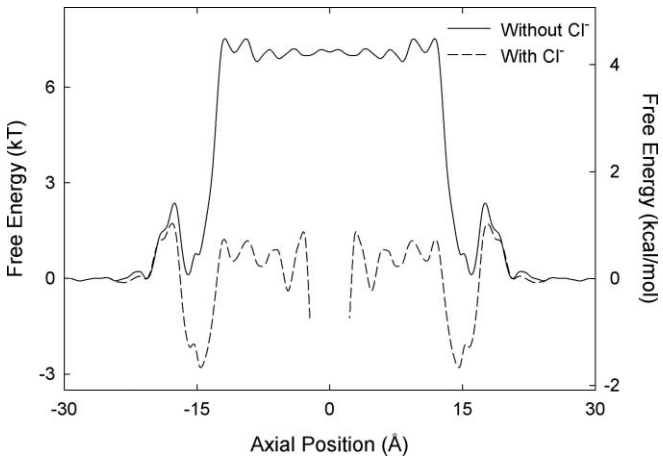

FIG. 6. One-dimensional free energy profile of sodium ions through the (10, 10) carbon nanotube with carboxylic acid terminated ends with (i) no chloride ions (Cl^-) present and (ii) a chloride ion fixed at $z = 0$ Å.

center or z = 0 Å, reduces the energy barrier encountered by an approaching sodium ion. When no chloride ion is present a sodium ion encounters an energy barrier of approximately 7 kT. However, the sodium ion no longer experiences an energy barrier when a chloride ion is present in the nanotube interior. Instead, the energy well at the nanotube entrance and exit increases from 2 to 4.5 and these wells are separated by a central barrier of approximately 4 kT. A free energy barrier of 2 kT remains for a sodium ion to enter the entrance or exit binding sites.

IV. CONCLUSION

In summary, we show that a (10, 10) carbon nanotube with an effective radius of 5.08 Å and a length of 36 Å terminated with carboxylic acid (COOH) are selective to sodium ions despite both sodium and chloride encountering an energy barrier of 7 kT to enter the nanotube. We find that chloride ions act as chaperones for sodium ions. The nanotube has a sodium conductance of 124 pS, and a negligible chloride conductance of 5 pS. Once inside the nanotube interior, chloride ions ferry sodium ions from the entrance to the exit. This artificial channel resembles that of the mutant glycine receptor[39] in which anions act to chaperone sodium ions with a conductance of 17 pS. This work illustrates the danger of relying solely on the single particle free energy profile to form a physical insight into the ion conduction mechanisms.

ACKNOWLEDGMENTS

We acknowledge the support from the National Health and Medical Research Council and the MAWA Trust. We thank Rhys Hawkins from the Visualization Laboratory at the Australian National University. The calculations upon which this work is based were carried out using the Sun X6275 blades cluster of the Australian National University Supercomputer Facility. We thank Associate Professor Michelle Coote and Junming Ho for helpful discussions.

[1]F. Fornasiero, H. G. Park, J. K. Holt, M. Stadermann, C. P. Grigoropoulos, A. Noy, and O. Bakajin, Proc. Natl. Acad. Sci. U. S. A. **105**, 17250 (2008).
[2]J. Hummer, J. C. Rasaiah, and J. P. Noworyta, Nature **414**, 188 (2001).
[3]A. Waghe, J. C. Rasaiah, and G. J. Hummer, Chem. Phys. **117**, 10789 (2002).
[4]A. Kalra, S. Garde, and G. Hummer, Proc. Natl. Acad. Sci. U. S. A. **100**, 10175 (2003).
[5]B. Corry, J. Phys. Chem. B **112**, 1427 (2008).
[6]J. A. Garate, N. J. English, and J. M. D. MacElroy, Mol. Simulat. **35**, 2 (2009).
[7]T. A. Hilder, D. Gordon, and S. H. Chung, Small **5**, 2183 (2009).
[8]C. Peter and G. Hummer, Biophys. J. **89**, 2222 (2005).
[9]S. Joseph, R. J. Mashl, E. Jakobsson, and N. R. Aluru, Nano Lett. **3**, 1399 (2003).
[10]M. Majumder, N. Chopra, and B. J. Hinds, J. Am. Chem. Soc. **127**, 9062 (2005).
[11]J. H. Park, S. B. Sinnott, and N. R. Aluru, Nanotech. **17**, 895 (2006).
[12]T. A. Hilder, D. Gordon, and S. H. Chung, Small **5**, 2870 (2009).
[13]C. Y. Won and N. R. Aluru, Chem. Phys, Lett. **478**, 185 (2009).
[14]T. A. Hilder, D. Gordon, and S. H. Chung, Biophys. J. **99**, 1734 (2010).
[15]C. Y. Lee, W. Choi, J. H. Han, and M. S. Strano, Science **329**, 1320 (2010).
[16]T. Lin, V. Bajpai, T. Ji, and L. Dai, Aust. J. Chem. **56**, 635 (2003).
[17]J. L. Bahr and J. M. Tour, J. Mater. Chem. **12**, 1952 (2002).
[18]D. Tasis, N. Tagmatarchis, V. Georgakilas, and M. Prato, Chem. Eur. J. **9**, 4000 (2003).
[19]C. F. Lopez, S. O. Nielsen, P. B. Moore, and M. L. Klein, Proc. Natl. Acad. Sci. U. S. A. **101**, 4431 (2004).
[20]D. Gordon, V. Krishnamurthy, and S. H. Chung, J. Chem. Phys. **131**, 134102 (2009).
[21]M. Hoyles, S. Kuyucak, and S. H. Chung, Phys. Rev. E **58**, 3654 (1998).
[22]M. S. Dresselhaus, G. Dresselhaus, and R. Saito, Carbon **33**, 883 (1995).
[23]B. R. Brooks, R. E. Bruccoleri, B. D. Olafson, D. J. States, S. Swaminathan, and M. J. Karplus, Comput. Chem. **4**, 187 (1983); A. D. MacKerell, Jr, B. Brooks, C. L. Brooks III, L. Nilsson, B. Roux, Y. Won, and M. Karplus, in *The Encyclopedia of Computational Chemistry*, edited by PvR Schleyer *et al.*, Vol. **1**, pp. 271–277 (John Wiley & Sons, Chichester), (1998).
[24]J. Zheng, E. M. Lennon, H. K. Tsao, and S. Jiang, J. Chem. Phys. **122**, 214702 (2005).
[25]K. M. Ranatunga, I. H. Shrivastava, G. R. Smith, and M. S. P. Sansom, Biophys. J. **80**, 1210 (2001).
[26]C. Adcock, G. R. Smith, and M. S. P. Sansom, Biophys. J. **75**, 1211 (1998).
[27]K. J. Ziegler, Z. Gu, J. Shaver, Z. Chen, E. L. Flor, D. J. Schmidt, C. Chan, R. H. Hauge, and R. E. Smalley, Nanotechnology **16**, S539 (2005).
[28]S. Wang, Z. Liang, B. Wang, C. Zhang, and Z. Rahman, Nanotechnology **18**, 055301 (2007).
[29]L. Kalé, R. Skeel, M. Bhandarkar, R. Brunner, A. Gursoy, N. Krawetz, J. Phillips, A. Shinozaki, K. Varadarajan, and K. Schulten, J. Comput. Phys. **151**, 283 (1999).
[30]W. Humphrey, A. Dalke, and K. Schulten, J. Molec. Graphics **14**, 33 (1996).
[31]M. A. Kastenholz and P. H. Hünenberger, J. Phys. Chem. B **108**, 774 (2004).
[32]S. Kumar, J. M. Rosenberg, D. Bouzida, R. H. Swendsen, and P. A. Kollman, J. Comput. Chem. **16**, 1339 (1995); A. Grossfield, http://membrane.urmc.rochester.edu/Software/ WHAM/WHAM.html [accessed 20 August 2008].
[33]H. J. C. Berendsen, *Simulating the Physical World: Hierarchical Modeling from Quantum Mechanics to Fluid Dynamics* (Cambridge University Press, Cambridge, 2007).
[34]D. Gordon, V. Krishnamurthy, and S. H. Chung, Molecular Physics **106**, 1353 (2008).
[35]L. G. Nilsson and J. A. Padró, Molecular Physics **71**, 355 (1990).
[36]S. Z. Wan, C. X. Wang, and Y. Y. Shi, Molecular Physics **93**, 901 (1998).
[37]R. Toghraee, R. J. Mashl, K. I. Lee, E. Jakobsson, and U. Ravaioli, J. Comput. Electron. **8**, 98 (2009).
[38]J. A. Ng, T. Vora, V. Krishnamurthy, and S. H. Chung, Biophys. J. **37**, 213 (2008).
[39]M. O'Mara, P. H. Barry, and S. H. Chung, Proc. Natl. Acad. Sci. U. S. A. **100**, 4310 (2003).
[40]S. Sugiharto, T. M. Lewis, A. J. Moorhouse, P. R. Schofield, and P. H. Barry, Biophys. J. **95**, 4698 (2008).
[41]P. H. Barry, S. Sugiharto, T. M. Lewis, and A. J. Moorhouse, Channels **4**, 142 (2010).